Supplementary materials for *Hemp pollen dispersal across the United States*

Manu Nimmala[1,*], Shane D. Ross[2+], and Hosein Foroutan[3+]

[1]Virginia Tech, Engineering Science and Mechanics, Blacksburg, Virginia 24061, USA
[2]Virginia Tech, Aerospace and Ocean Engineering, Blacksburg, Virginia 24061, USA
[3]Virginia Tech, Civil and Environmental Engineering, Blacksburg, Virginia 24061, USA
[*]nimmala@vt.edu
[+]these authors contributed equally to this work

S-1 Supplementary Methods

S-1.1 Model Formulation

The Lagrangian Stochastic (LS) model is an application of Brownian motion to turbulent diffusion, in which the trajectories of many particles through the air are modeled as random walks. Each step of a particle's path is influenced by both random and deterministic motions, guided by the statistics of the local wind field. By releasing thousands of particles and computing an ensemble average of their trajectories, we can determine the relative concentration at any point in the domain and the mean shape of the plume.

In this study, we implement two LS model formulations for the Eulerian velocity pdf: a convective boundary layer (CBL) model for unstable conditions ($L < 0$)[1,2] and a surface layer (SL) model for stable conditions[3] ($L > 0$), where L is the Monin-Obukhov length.

The position increments for particles in the x (downwind) and z (vertical) directions are as follows[3],

$$dx = (u' + \overline{U})dt, \tag{1}$$
$$dz = (w' - v_s)dt, \tag{2}$$

where u' and w' represent the fluctuating horizontal and vertical velocities, $\overline{U}$ is the mean horizontal wind velocity described further in Section S-1.2.1, and v_s is a constant settling velocity for hemp computed using Stoke's law to be 0.027 m/s based on a typical hemp pollen diameter of 30 μm[4,5]. As hemp pollen is nearly spherical[5], Stoke's law provides a good approximation of settling velocity[6,7].

Particle velocity increments[3] in the x and z directions are computed using the Langevin equation,

$$du' = a_u dt + b_u \mathcal{N}(0, dt), \tag{3}$$
$$dw' = a_w dt + b_w \mathcal{N}(0, dt), \tag{4}$$

which describes the incremental changes in u' and w' fluctuating particle velocities. The Langevin coefficients, a_u, a_w and b_u, b_w, account for the deterministic and stochastic components of particle acceleration, respectively. The stochastic timestep is drawn from a normal distribution with a mean of 0 and variance dt.

The timestep, dt is computed as a fraction[1,3] of the lagrangian timescale τ:

$$dt = 0.02\tau, \tag{5}$$
$$\tau = 2\frac{\sigma_w^2}{C_0\varepsilon}, \tag{6}$$

where we chose the constant $C_0 = 3$[8,9], σ_w^2 is the vertical velocity variance and ε is the turbulent dissipation rate.

The two model formulations employed differ in their computation of the Langevin coefficients a_u and a_w, and particularly in how they solve for the Eulerian fluid velocity pdf $P_E(u_i', z)$ in the equations[10] below.

$$a_i = \frac{\phi_i}{P_E} + \frac{\frac{1}{2}C_0\varepsilon\frac{\partial P_E}{\partial u_i}}{P_E}, \tag{7}$$
$$b_i = \sqrt{C_0\varepsilon}. \tag{8}$$

For both formulations, b_u and b_w remain the same as above.

S-1.1.1 The Convective Boundary Layer (CBL) model for unstable conditions ($L < 0$)

The CBL model was introduced by Luhar et al. (1989)[11], and computes $P_E(u_i', z)$ as the sum of two Gaussian pdfs to represent convective updrafts and downdrafts in the boundary layer, shown in (9),

$$\begin{aligned} P_E &= AP_A + BP_B, \\ P_A &= \frac{1}{\sqrt{2\pi}\sigma_A} \exp\left(\frac{-(w' - \overline{w}_A)^2}{2\sigma_A^2}\right), \\ P_B &= \frac{1}{\sqrt{2\pi}\sigma_B} \exp\left(\frac{-(w' + \overline{w}_B)^2}{2\sigma_B^2}\right). \end{aligned} \tag{9}$$

It is extended to 2 dimensions based on Luhar (2002)[8,9], which takes the horizontal and vertical velocity fluctuations to be independent. The Langevin coefficients then become,

$$a_w = \frac{\phi}{P_E} - \frac{\frac{1}{2}C_0\varepsilon Q}{P_E}, \tag{10}$$

$$a_u = \frac{-u' C_0 \varepsilon}{2\sigma_u^2}. \tag{11}$$

The ϕ term has been adapted to heavy particles in Boehm et al. (2005)[2]. The full closure method to find A, B, $\overline{w_A}$, $\overline{w_B}$, σ_A, σ_B is shown in Luhar et al. (1996)[1]. These are functions of the wind velocity profiles, which vary with height and are described in Section S-1.2. Although the original CBL LS model[1,11] was a one-dimensional model intended for the well-mixed boundary-layer, Boehm et al. (2008)[8] incorporated wind statistics into this model which transition smoothly from the surface layer to the convective boundary layer above.

S-1.1.2 Surface Layer LS Model for Stable Conditions ($L > 0$)

For stable conditions, the SL model incorporates a Gaussian pdf (eq. (12)) with jointly Gaussian velocity components (u, v, and w), as described in[3,10,12], giving a P_E,

$$P_E = \frac{1}{(2\pi)^{3/2} \det \tau_{ij}^{1/2}} \exp\left(-\frac{1}{2}(u_i - U_i)\tau_{ij}^{-1}(u_j - U_j)\right). \tag{12}$$

where τ_{ij} is the mean Reynold's stress tensor, and contains terms for the variances and covariances of the wind velocity.

This yields the Langevin coefficients used in Aylor & Flesch (2001)[3].

$$a_u = \frac{1}{A} b_u^2 (\overline{u'w'}w' - \sigma_w^2 u') + \frac{1}{2}\frac{\partial \overline{u'w'}}{\partial z} + \frac{1}{A}(\sigma_w^2 \frac{\partial \sigma_u^2}{\partial z} u'w' - \overline{u'w'}\frac{\partial \sigma_u^2}{\partial z} w'^2 - \overline{u'w'}\frac{\partial \overline{u'w'}}{\partial z} u'w' + \sigma_u \frac{\partial \overline{u'w'}}{\partial z} w'^2), \tag{13}$$

$$a_w = \frac{1}{A} b_w^2 (\overline{u'w'}u' - \sigma_u^2 w') + \frac{1}{2}\frac{\partial \sigma_w^2}{\partial z} + \frac{1}{A}(\sigma_w^2 \frac{\partial \overline{u'w'}}{\partial z} u'w' - \overline{u'w'}\frac{\partial \overline{u'w'}}{\partial z} w'^2 - \overline{u'w'}\frac{\partial \sigma_w^2}{\partial z} u'w' + \sigma_u^2 \frac{\partial \sigma_w^2}{\partial z} w'^2), \tag{14}$$

$$A = 2(\sigma_u^2 \sigma_w^2 - \overline{u'w'}^2). \tag{15}$$

S-1.2 Wind statistics

To compute the Eulerian velocity pdf $P_E(u_i', z)$, we need to specify the wind statistics at every point in the domain, i.e., the mean, variances, covariances, and skewness. Assuming stationarity and horizontal homogeneity, the wind field statistics remain constant over time and vary only with height. Under this assumption, boundary layer scaling techniques such as Monin-Obukhov similarity theory, mixed layer, and surface layer scaling can be employed to generate vertical profiles of wind statistics. As a result, only 5 meteorological parameters are required to drive the LS simulation: the friction velocity u^*, the Monin-Obukhov length L, the convective velocity scale w^*, the surface roughness length z_0, and boundary layer height z_i.

S-1.2.1 Horizontal wind velocity profile

To model the mean horizontal wind-velocity profile, $\overline{U}$, we use the logarithmic wind velocity profile from Monin-Obukhov similarity theory[13] with the stability correction function, ψ_M.

$$\overline{U} = \frac{u^*}{0.4}\left[\ln\left(\frac{z}{z_0}\right) + \psi_M\right]. \tag{16}$$

For stable conditions, we use the stability function as reported in Beljaars & Holtslag (1991)[14], where $a = 1$, $b = 2/3$, $c = 5$, and $d = 0.35$. In this paper, they compare the resulting velocity profiles with field measurements and find that this parameterization performs well throughout the boundary layer despite the fact that surface-layer scaling is used. Optis et al. (2016)[15] also compared various stable wind profiles, including the one presented below, and show that it performs well up to 200 meters above the surface.

$$\psi_M = a\frac{z}{L} + b\left(\frac{z}{L} - \frac{c}{d}\right)\exp\left(-d\frac{z}{L}\right) + \frac{bc}{d}. \tag{17}$$

For unstable conditions, we use the stability function given by Paulson (1970)[16]. This has previously been used for other unstable LS simulations[3,8], and is considered to approximate measurements well[14].

$$\psi_M = -2\ln\left(\frac{1+\alpha}{2}\right) - \ln\left(\frac{1+\alpha^2}{2}\right) + 2\tan^{-1}(\alpha) - \frac{\pi}{2}, \tag{18}$$

where,

$$\alpha = (1 - 15\frac{z-d}{L})^{1/4}. \tag{19}$$

S-1.2.2 Horizontal wind velocity variance

In stable conditions, we use the following relationship from Kantha and Clayson for the horizontal velocity variance (2000)[17],

$$\sigma_u^2 = 4u^{*2}\left(1 - \frac{z}{z_i}\right)^{3/2}. \tag{20}$$

In unstable conditions, we use the following parameterization from Luhar et al. (2002)[9] for the horizontal wind velocity variance.

$$\sigma_u^2 = (0.6w^*)^2. \tag{21}$$

S-1.2.3 Vertical wind velocity variance

In stable conditions, for the vertical wind velocity variance, we use a relationship from Kantha and Clayson[17],

$$\sigma_w^2 = 3u^{*2}\left(1 - \frac{z}{z_i}\right)^{3/2}. \tag{22}$$

In the HYSPLIT model, this parameterization is provided as one option for simulating velocity variances in stable conditions. Oneto et al. (2020) compared dispersal results using the Kantha and Clayson (2000) scheme with other parameterizations offered by HYSPLIT, and found that there was little sensitivity.

In unstable conditions, we apply the merged parameterization from Boehm et al. (2005)[8]. This combines surface-layer scaling with that of the convective boundary layer, so that the conditions ranging from very unstable to neutral can be accurately modeled.

$$\sigma_{w,CBL}^2 = 1.7w^{*2}(z/z_i)^{2/3}(1 - 0.9z/z_i)^{4/3}, \tag{23a}$$

$$\sigma_{w,neutral}^2 = u^{*2}(1.7 - z/z_i), \tag{23b}$$

$$\sigma_{w,merged}^2 = \frac{(1-\exp(z/L))w^{*3}\sigma_{w,CBL}^2 + 5\exp(z/L)u^{*3}\sigma_{w,neutral}^2}{(1-\exp(z/L))w^{*3} + 5\exp(z/L)u^{*3}}. \tag{23c}$$

(23d)

S-1.2.4 Turbulence kinetic energy dissipation rate

In stable conditions, we use the profile suggested by Rodean (1996)[10] for the entire stable boundary layer,

$$\varepsilon = \frac{u^{*3}}{0.4 * z}\left(1 + 3.5\frac{z}{L}\right)\left(1 - 0.85 * \frac{z}{z_i}\right)^{3/2}. \tag{24}$$

Rodean (1996) discusses that this profile was formed by fitting to a second-order turbulence model[18], and has generally agreed with measurements and other simulations.

In unstable conditions, we apply the merged surface layer/convective boundary layer profile described by Boehm et al. (2008)[8] to LS modeling, and found previously using Large Eddy Simulations[19],

$$\varepsilon = 0.4\frac{w^{*3}}{z_i} + \frac{u^{*3}(1 - z/z_i)}{0.4z(1 - 15 * z/L)^{1/4}}. \tag{25}$$

S-1.2.5 Lagrangian Timescale

In all stabilities, we compute the lagrangian time scale using[1,3],

$$\tau = \frac{2\sigma_w^2}{C_0\varepsilon}. \tag{26}$$

Figure S1

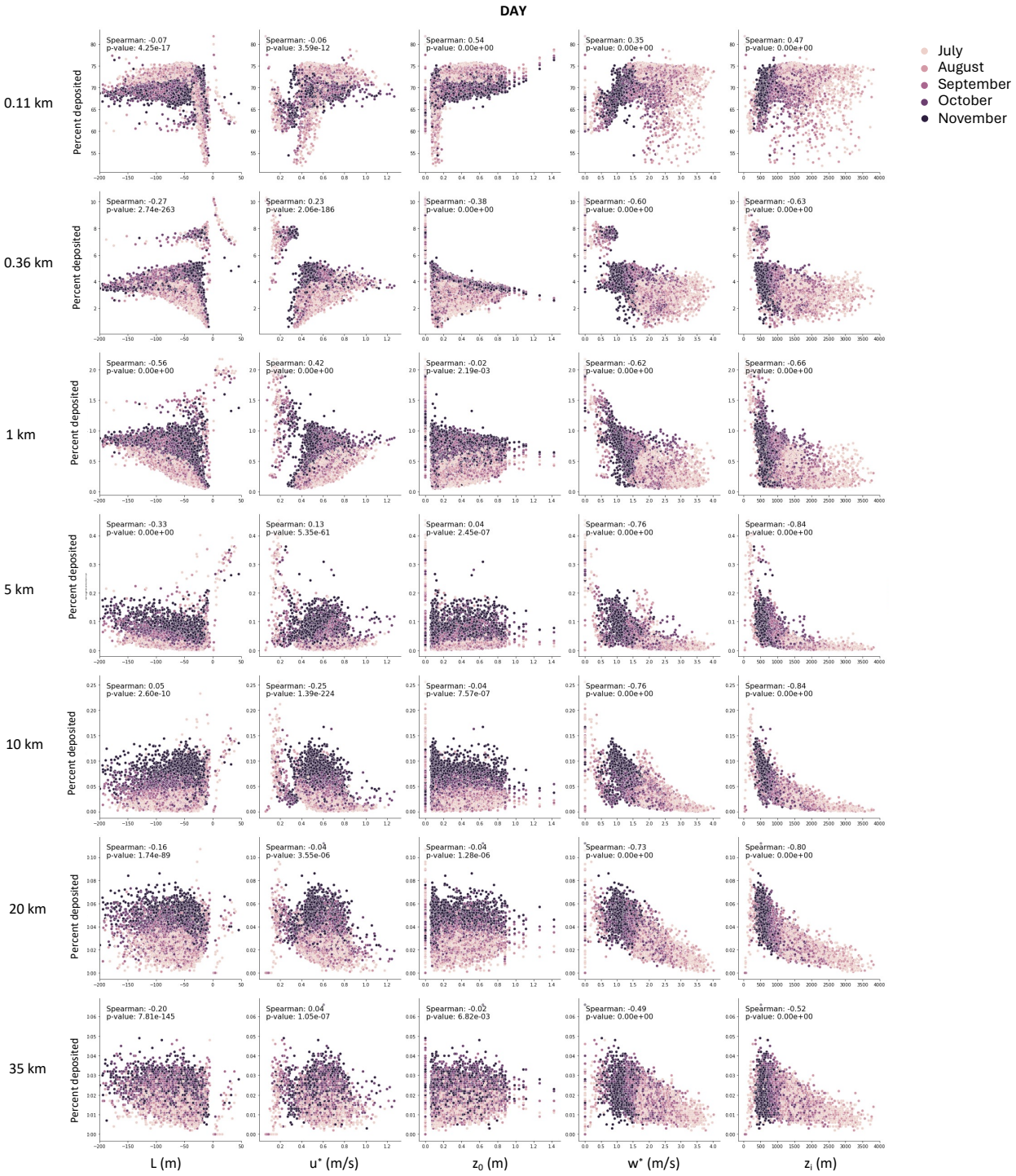

Figure S-1. Scatterplots of five meteorological parameters for all day simulations vs. the percentage of particles deposited at distances downwind of the source. The Spearman correlation coefficients relating depositions at each downwind distance with the respective meteorological parameter are denoted for each plot. Decreasing deposition is most correlated with decreased boundary layer height z_i and w^* beyond 1 km from the source.

Figure S2

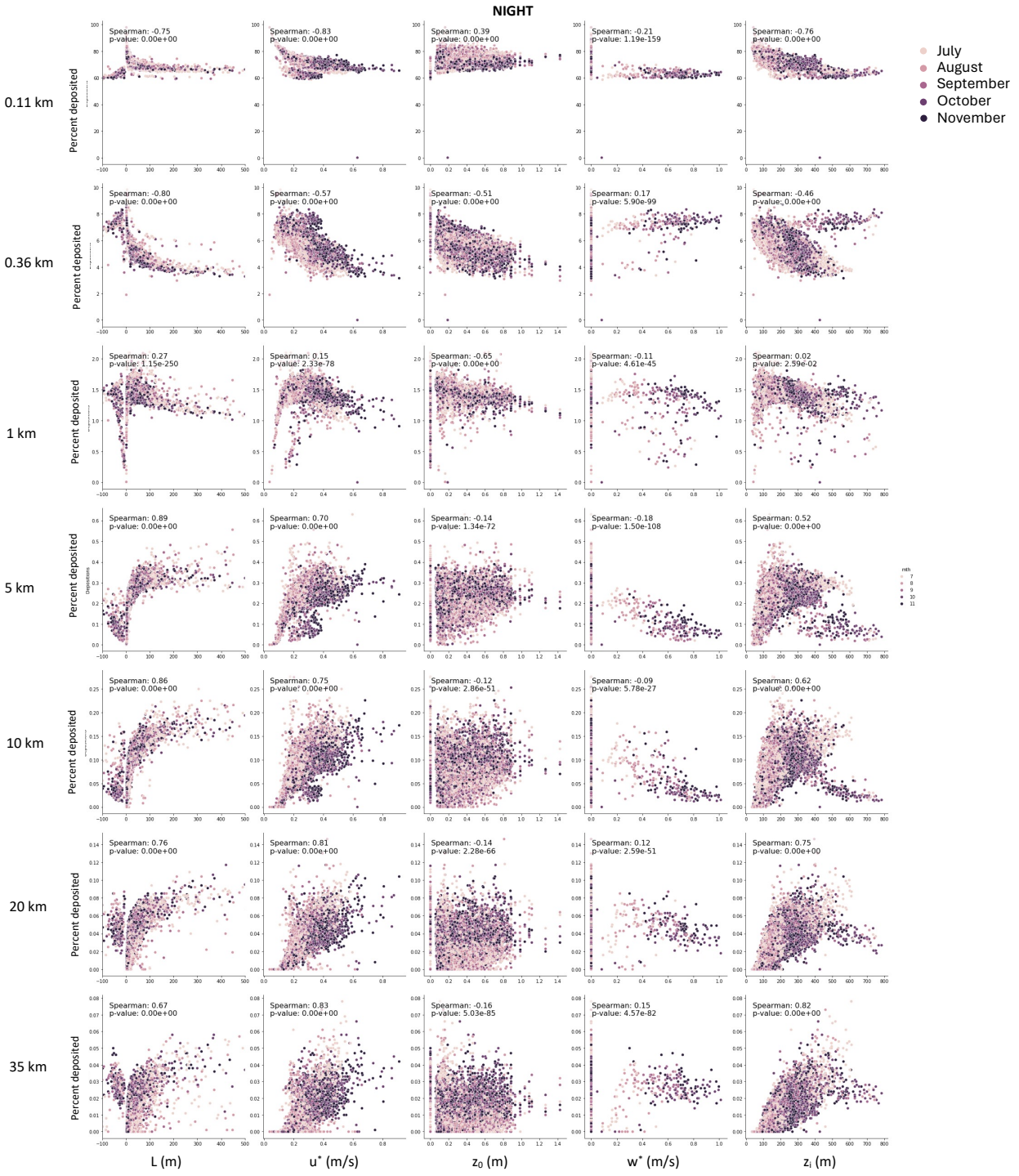

Figure S-2. Scatter plots of meteorological input parameters vs. depositions for night cases. Scatterplots of five meteorological parameters for all **night** simulations vs. the percentage of particles deposited at distances downwind of the source. The Spearman correlation coefficients relating depositions at each downwind distance with the respective meteorological parameter are denoted for each plot. At night, greater boundary layer height z_i, friction velocity u^*, and obukhov length $|L|$ correlate with pollen travelling further - less deposition close to the source and increased deposition at all downwind distances beyond 1 km. The convective velocity scale, w^* is zero or a very small negative number for all night-time conditions, which make up the vast majority of nighttime case, and is not incorporated in the stable LS model.

Figure S3

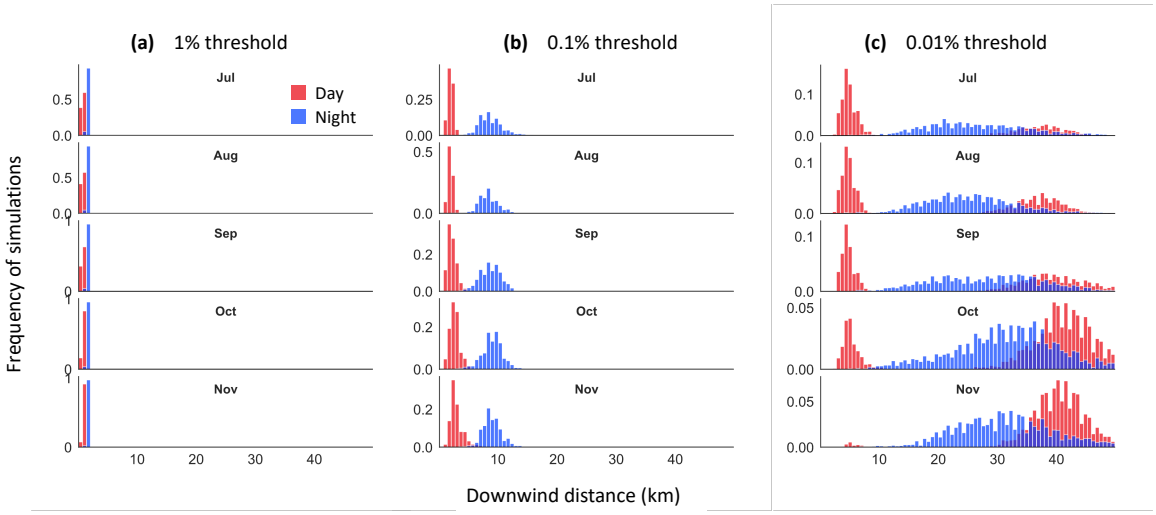

Figure S-3. Distances at which dispersal kernels first fall below a threshold for each month: (a) 1%, (b) 0.1%, and (c) 0.01%. Red represents day simulations, while blue represents night. Seasonal variation is most pronounced for the 0.01% threshold distances, where the frequency of daytime distances beyond 30 km progressively increases from July to November.

Figure S4

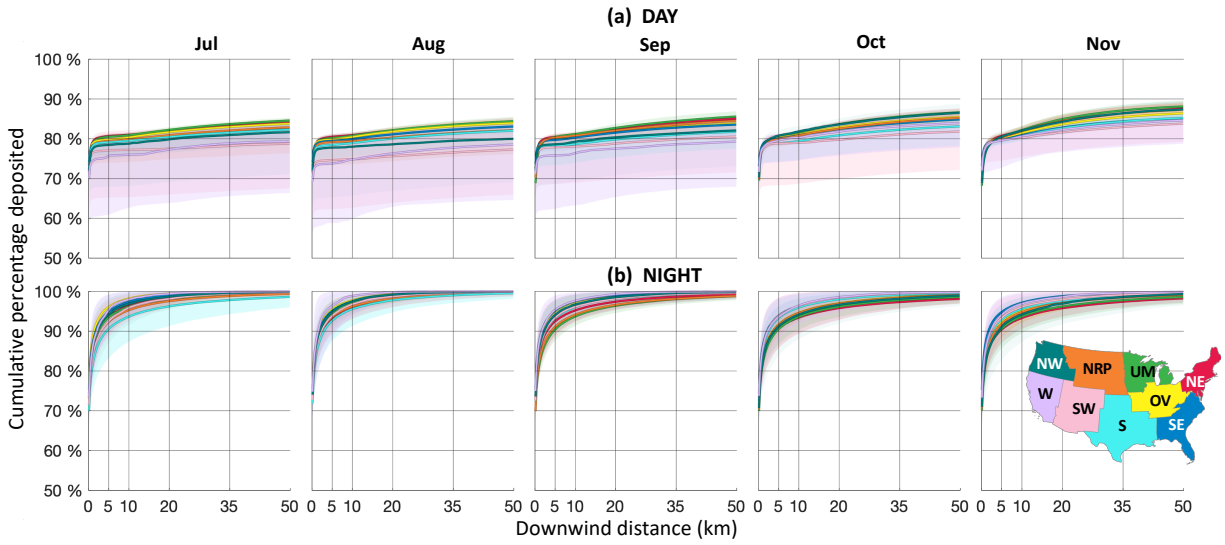

Figure S-4. Median cumulative depositions for each month during (a) day and (b) night, separated by US climate region: Northeast (NE), Upper Midwest (UM), Ohio Valley (OV), Southeast (SE), Northern Rockies & Plains (NRP), South (S), Southwest (SW), Northwest (NW), and West (W). Shading represents data between the 10th and 90th percentiles. Note that the vertical axis is a log scale. There is a pronounced increase in total depositions in nighttime cases - most curves reach 100% within the domain. During the day, the kernels level out below 90%, although there is an increase in depositions from July to November.

Figure S5

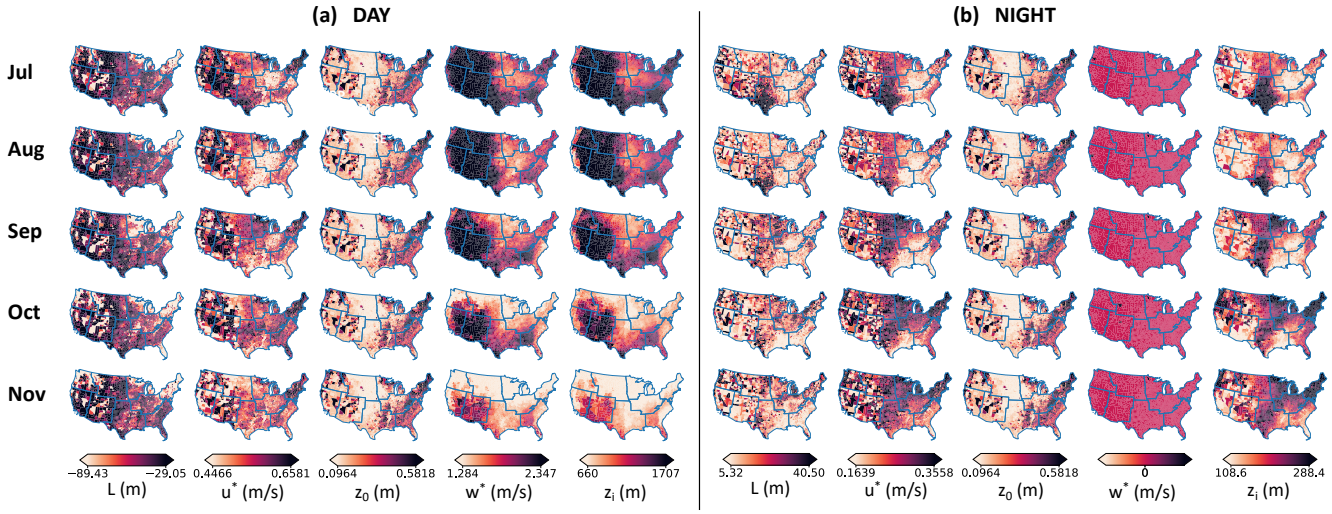

Figure S-5. Heat maps of five meteorological parameters for all (a) daytime and (b) nighttime simulations over five months from July to November. The spatial and seasonal patterns visualized here mirror the deposition patterns shown in the main paper. During the day, the Southwest region maintains the highest convective velocity scale, w^* and boundary layer height, z_i throughout the season, and therefore the lowest daytime depositions overall. At night, the Southeast and Southwest regions have high friction velocity, u^*, high boundary layer height, z_i, lower roughness length, z_0, and high Monin-Obukhov length $|L|$, which results in less deposition in our simulations.

Figure S6

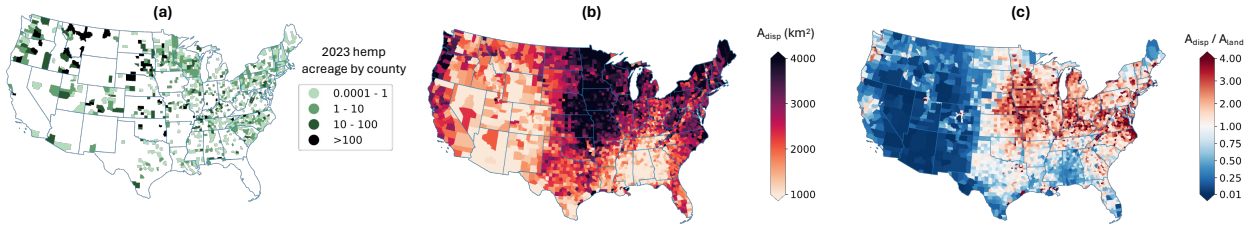

Figure S-6. Components of the vulnerability metric. (a) The acreage of hemp, A_{hemp}, planted in each county as of 2023[20], where darker colors indicate greater planted hemp acreage. (b) The dispersal area A_{disp}, or area within a circle of radius equal to the average 0.01%-threshold distance, where darker colors indicate a greater dispersal area. (c) The ratio of A_{disp} to the land area of each county A_{land}, where red colors indicate regions where more $A_{disp} > A_{land}$.

Supplementary References

1. Luhar, A. K., Hibberd, M. F. & Hurley, P. J. Comparison of closure schemes used to specify the velocity pdf in lagrangian stochastic dispersion models for convective conditions. *Atmospheric Environ.* **30**, 1407–1418 (1996).
2. Boehm, M. T. & Aylor, D. E. Lagrangian stochastic modeling of heavy particle transport in the convective boundary layer. *Atmospheric Environ.* **39**, 4841–4850 (2005).
3. Aylor, D. E. & Flesch, T. K. Estimating spore release rates using a lagrangian stochastic simulation model. *J. Appl. Meteorol. Climatol.* **40**, 1196–1208 (2001).
4. Small, E. & Antle, T. A preliminary study of pollen dispersal in cannabis sativa in relation to wind direction. *J. Ind. Hemp* **8**, 37–50 (2003).
5. Clarke, R. C. *Botany of the Genus Cannabis* (Haworth Press, Binghamton, NY, 1999).

6. Borrell, J. S. Rapid assessment protocol for pollen settling velocity: Implications for habitat fragmentation. *Biosci. Horizons* **5**, 1–9, DOI: 10.1093/biohorizons/hzs002 (2012).

7. Aylor, D. *Aerial Dispersal of Pollen and Spores* (American Phytopathological Society, 2017).

8. Boehm, M. T., Aylor, D. E. & Shields, E. J. Maize pollen dispersal under convective conditions. *J. Appl. Meteorol. Climatol.* **47**, 291–307 (2008).

9. Luhar, A. K. The influence of vertical wind direction shear on dispersion in the convective boundary layer, and its incorporation in coastal fumigation models. *Boundary-Layer Meteorol.* **102**, 1–38, DOI: 10.1023/A:1012710118900 (2002).

10. Rodean, H. C. *Stochastic Lagrangian Models of Turbulent Diffusion*, vol. 6 (1996).

11. Luhar, A. K. & Britter, R. E. A random walk model for dispersion in inhomogeneous turbulence in a convective boundary layer. *Atmospheric Environ. (1967)* **23**, 1911–1924 (1989).

12. Thomson, D. J. Criteria for the selection of stochastic models of particle trajectories in turbulent flows. *J. Fluid Mech.* **180**, 529–556, DOI: 10.1017/S0022112087001940 (1987).

13. Stull, R. B. An introduction to boundary layer meteorology. *An introduction to boundary layer meteorology* (1988).

14. Beljaars, A. & Holtslag, A. Flux parameterization over land surfaces for atmospheric models. *J. Appl. Meteorol. Climatol.* **30**, 327–341 (1991).

15. Optis, M., Monahan, A. & Bosveld, F. C. Limitations and breakdown of monin–obukhov similarity theory for wind profile extrapolation under stable stratification. *Wind. Energy* **19**, 1053–1072 (2016).

16. Paulson, C. A. The mathematical representation of wind speed and temperature profiles in the unstable atmospheric surface layer. *J. Appl. Meteorol. Climatol.* **9**, 857–861 (1970).

17. Kantha, L. H. & Clayson, C. A. *Small scale processes in geophysical fluid flows* (Elsevier, 2000).

18. Brost, R. & Wyngaard, J. A model study of the stably stratified planetary boundary layer. *J. Atmospheric Sci.* **35**, 1427–1440 (1978).

19. Moeng, C.-H. & Sullivan, P. P. A comparison of shear-and buoyancy-driven planetary boundary layer flows. *J. Atmospheric Sci.* **51**, 999–1022 (1994).

20. Agency, F. S. FSA Crop Acreage Data Reported to FSA, 2023 acreage data as of August 9, 2023 (2023).